A novel algorithm to resolve lack of convergence and checkerboard instability in bone adaptation simulations using non-local averaging

José Luis Calvo-Gallego[a,*], Peter Pivonka[b], José Manuel García-Aznar[c], Javier Martínez-Reina[a]

[a] *Departmento de Ingeniería Mecánica y Fabricación, Universidad de Sevilla, Seville 41092, Spain*
[b] *School of Mechanical, Medical and Process Engineering, Queensland University of Technology, QLD 4000, Australia.*
[c] *M2BE-Multiscale in Mechanical and Biological Engineering, Instituto de Investigación en Ingeniería de Aragón (I3A), Instituto de Investigación Sanitaria Aragón (IIS Aragón), Universidad de Zaragoza, Zaragoza, Spain*

Abstract

Checkerboard is a typical instability in finite element (FE) simulations of bone adaptation and topology optimization in general. It consists in a patchwork pattern with elements of alternating stiffness, producing lack of convergence and instabilities in the predicted bone density. Averaging techniques have been proposed to solve this problem. One of the most acknowledged techniques (node based formulation) has severe drawbacks such as: high sensitivity to mesh density and type of element integration (full vs. reduced) and, more importantly, oscillatory solutions also leading to lack of convergence. We propose a new solution consisting in a non-local smoothing technique. It defines, as the mechanical stimulus governing bone adaptation in a certain integration point of the mesh, the average of the stimuli obtained in the neighbour integration points. That average is weighted with a decay function of the distance to the centre of the neighbourhood. The new technique has been shown to overcome all the referred problems and perform in

*Corresponding author: joselucalvo@us.es
Email addresses: peter.pivonka@qut.edu.au (Peter Pivonka), jmgaraz@unizar.es (José Manuel García-Aznar), jmreina@us.es (Javier Martínez-Reina)

This article has been accepted for publication and undergone full peer review but has not been through the copyediting, typesetting, pagination and proofreading process which may lead to differences between this version and the Version of Record. Please cite this article as doi: 10.1002/cnm.3419

a robust way. It was tested on a hollow cylinder, resembling the diaphysis of a long bone, subjected to bending or torsion. Checkerboard instability was eliminated and local convergence of bone adaptation was achieved rapidly, in contrast to the other averaging technique and to the model without control of checkerboard instability. The new algorithm was also tested with good results on the same geometry but in a model containing a void, which produces a stress concentration that usually leads to checkerboard instability, like in other applications such as simulations of bone-implant interfaces.

Keywords: Bone adaptation; Mechanostat Theory; FE analysis; checkerboard; topology optimization; convergence

1. Introduction

Checkerboard patterns typically occur in finite element (FE) simulations of different applications, such as damage localisation [1, 2] or topology optimization [3, 4]. Damage localisation is a common problem in Continnum Damage Mechanics (CDM), which has also been extended to bone remodelling applications [5]. In both cases, a localisation issue is present, which controls the local constitutive law leading to ill-posed problems [6]. Different approaches have been proposed to solve this localization problem, such as, the introduction of gradients of the displacement [7], strain and/or internal variable fields by means of phenomenological considerations [2] or derived through homogenisation (see, e.g., [8]) or the diffusion of apparent density [6].

Topology optimization aims to find an optimal structure that can bear certain loads with the minimum weight. The optimization procedure usually delivers a patchwork pattern with elements of alternating high and low stiffness, commonly referred to as checkerboard instability. As stated by Fyhrie and Carter [9], bone is an optimum structure in that same sense, since its microstructure is organized such that it can bear daily loads with a minimum structural weight. Furthermore, bone can adapt itself to changes in the applied (external) loads through a process referred to as bone adaptation, so keeping the optimality condition [10]. In fact, these authors termed bone as a self-optimizing material. For this reason, checkerboard instability is commonly observed in FE simulations of bone adaptation studies [11].

In such simulations, bone density distribution is predicted as a function of external loads. This type of simulations uses the Mechanostat Theory

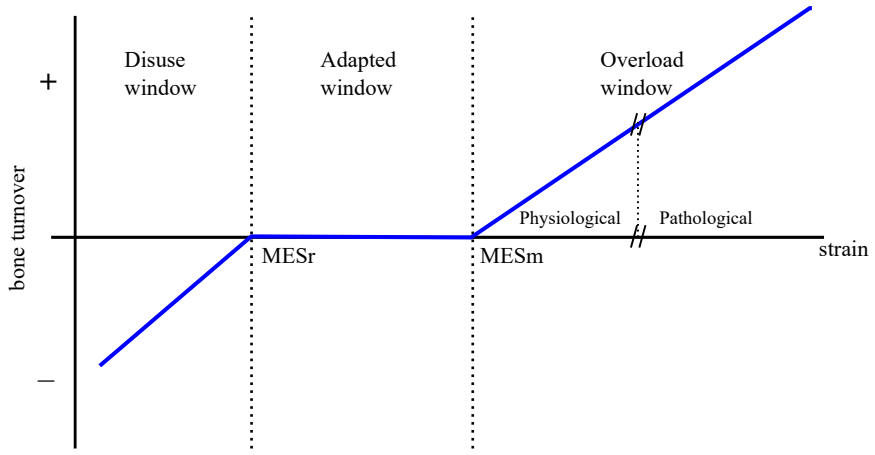

Figure 1: Schematic picture of the Mechanostat Theory (adapted from Frost [12]). In Frost's terminology, the thresholds $\mathrm{MES_r}$ and $\mathrm{MES_m}$ designate respectively the strain limit below which disuse-mode remodelling appears or above which overload modelling takes place.

[12], which establishes a direct relationship between loads and bone resorption/formation. This theory postulates the existence of a range of (equivalent) strain or mechanical stimulus ("Adapted window") within which bone is adapted and does not change its density (see Fig. 1). For a given applied (external) load, if the strain stimulus is larger than the minimum effective strain (MES_m), bone formation occurs and the bone density increases, thus making bone stiffer and so reducing strain in the bone matrix. On the contrary, if strain stimulus is below the minimum effective stain for resorption (MES_r), bone resorption occurs and density decreases, making bone more flexible and so increasing the strain in the bone matrix. In both cases, the evolution of density is such that bone "searches" for the Adapted window. In other words, bone density is dependent on the local strain stimulus and changes until its stiffness is such that local strain is within the Adapted window. FE simulations commonly start from an arbitrary density distribution assumed to be uniform across the domain [5, 13]. External loads are then applied to the FE model and, based on the implemented adaptation algorithm, bone density changes until an adaptation equilibrium state is reached with no further changes to occur [14].

However, that self-optimizing algorithm has been shown to lead to checkerboard instability, which in certain cases delivers a patchwork distribution of

bone density. According to Weinans et al. [15] the keypoint to discern if checkerboard instability appears is the relationship between bone apparent density (ρ) and bone stiffness, usually given by the Young's modulus as a function of bone density:

$$E = C\,\rho^{\gamma} \tag{1}$$

where C and γ are experimentally determined constants. More precisely, those authors showed that the adaptation equilibrium state is a saddle point if $\gamma > 1$. Therefore, different density distributions can be obtained depending on the initially assumed distribution, or if a perturbation arises. Fig. 2 shows the *two unit model* presented by Weinans et al. [15] to illustrate the perturbation problem. If this model is subjected to a constant strain state, $\varepsilon = \varepsilon_1 = \varepsilon_2$, the total applied stress is distributed such that $\sigma = \sigma_1 + \sigma_2 = E_1\,\varepsilon + E_2\,\varepsilon$ and the elements bear more load as they become stiffer (denser). Let us think of a uniform stress distribution leading to a uniform density distribution, $\rho = \rho_1 = \rho_2$. If a certain perturbation of density arises, $\delta\rho$, such that $\rho_1 = \rho + \delta\rho$ and $\rho_2 = \rho$, element 1 becomes stiffer than element 2 by virtue of Eq. (1) and attracts more load. For this reason, the Mechanostat theory would predict an increase of density in element 1 (see Fig. 1), so amplifying the perturbation. The difference between the densities of elements 1 and 2 would increase to deliver the typical patchwork distribution and making the model unstable.

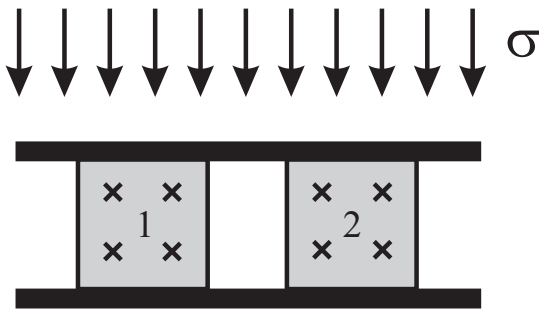

Figure 2: Two-unit adaptation model according to Weinans et al. [15]. Crosses indicate the position of integration points. The bottom plate is fixed and a uniform load is applied over the top plate.

The procedures that can be found in the literature to resolve checkerboard instability consist in applying smoothing techniques to enforce continuity of

density across elements. Weinans et al. [15] used a postprocessing technique consisting in extrapolating the element solution of density (potentially discontinuous) to the nodes using the element shape functions. Then, the different extrapolated values (one per element) were averaged at each node to achieve a continuous and smooth solution. The node-based formulation (NBF) proposed by Jacobs et al. [11] and Chen et al. [16] uses a similar procedure, though not implemented at the postprocessing stage. For the NBF, smoothing is not applied to the final result of bone density, but to the mechanical stimulus that drives bone adaptation. Subsequently, the bone adaptation algorithm is applied at the FE nodes, now with a smoothed distribution of mechanical stimulus, to obtain a density distribution which is consequently smooth and continuous.

In the current work we show that the NBF method has drawbacks that make it unsuitable under certain conditions. Among these: 1) the instability is not fully resolved and thus convergence is not ensured; 2) the solution is highly dependent on the mesh density; 3) convergence also depends on the type of FE integration (full or reduced). The objective of this paper is to present a new method to resolve checkerboard instability that overcomes the aforementioned drawbacks. The new method utilises a non-local smoothing technique, which is not constrained to the elements but applied to the neighbourhood of integration points, defined by a sphere of a given radius (R). This radius R must be chosen carefully to overcome the aforementioned convergence issues, but it can also be chosen to provide a deeper physiological meaning to the bone adaptation algorithm. In certain situations, it is not appropriate to simulate bone response in a very localised manner, since the cells responsible for bone adaptation (e.g. osteocytes) not only sense the local mechanical stimuli which is linked to a certain integration point or any other mathematical limitation. Instead, it is plausible to assume that those cells sense an average mechanical stimulus from their close vicinity, whose size will be dependent on the nature of that stimulus and the responsiveness of cells [17].

The paper is organized as follows: Section 2 describes the proposed method. In Section 3 the method is applied to a simple model: a cylindrical hollow bone subjected to bending and torsion loads. The results of the new method are compared with those obtained without correction of checkerboard instability and with the correction previously proposed in the literature, NBF. The performance of smoothing techniques is also evaluated in a model including a stress concentration. The comparison between

smoothing techniques is discussed in Section 4. Conclusions are presented in Section 5. The Appendix is devoted to a brief description of the bone adaptation algorithm and of the code used to implement the method, which is provided as Supplementary Material.

2. Materials and Methods

2.1. Bone adaptation algorithm

The method proposed in this paper is valid for any bone adaptation model (BAM) implementing the Mechanostat or a similar theory. On a general basis, BAMs yield the change of some state variables (apparent density in most cases, though other models, such as the one implemented here, give other variables, e.g. damage, mineral content, etc.) as a function of applied loads. Bone stiffness is correlated with these state variables using expressions obtained experimentally in order to update the stiffness at each iteration step. Here we use the following expression for bone stiffness as a function of the bone matrix volume fraction and the ash fraction given by Hernandez et al. [18]:

$$E(\text{MPa}) = 84370 \left(\frac{f_{bm}}{100}\right)^{2.58} \alpha^{2.74} (1-d) \tag{2}$$

where f_{bm} is the volume fraction of extravascular bone matrix, (equivalent to BV/TV, i.e. bone matrix volume per total volume, though in the case of f_{bm} expressed as a percentage), α is the ash fraction, a variable used to measure the mineral content of bone matrix, [19] and $d \in [0, 1]$ is a variable that measures microstructural damage and is related to degradation of stiffness, as introduced in classical damage mechanics [20, 21].

A general scheme of a typical bone adaptation algorithm not implementing the control of checkerboard instability is illustrated in Fig. 3. The simulation is initialised from an arbitrary distribution of the state variables (generally uniform). The iteration process applying the bone adaptation law (Mechanostat model) is repeated until convergence of state variables is achieved. Note that convergence speed also depends on the slopes of the formation and resorption regions (see Fig. 1). As seen in Eq. (2), the state variables of this model are: bone volume fraction, f_{bm}, mineral content, α, (both can provide apparent density) and microstructural damage, d. More details of the BAM used in this paper can be found in the Appendix.

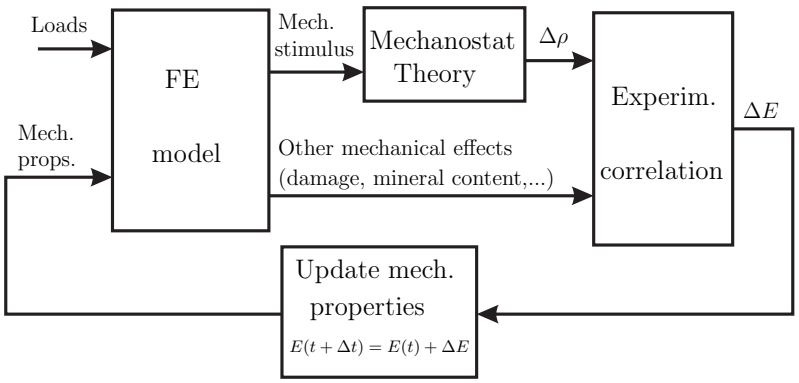

Figure 3: General scheme of a bone adaptation algorithm without control of checkerboard instability.

2.2. Node-based formulation (NBF)

Checkerboard instability occurs when convergence is not achieved and state variables either oscillate during the simulation at a given element or exhibit an alternating spatial distribution. To resolve that problem, Weinans et al. [15] proposed to use the smoothed nodal solution. This method consists in extrapolating the density element solution from the integration points to the nodes. As a node could have different extrapolated values (one per element sharing that node), an average of those extrapolated values is defined as the nodal density value.

Jacobs et al. [11] proposed a similar technique, termed as node-based formulation (NBF). These authors extrapolated the mechanical stimulus to the nodes and averaged the extrapolated values to obtain a nodal solution of the mechanical stimulus. Then, the Mechanostat theory was applied at the nodes in order to obtain a continuous density distribution.

2.3. Neighbourhood averaging method (NAM)

The method presented in this paper proposes a different averaging technique. For a given integration point, p, a neighbourhood of integration points, N, is defined by those ones contained in a sphere of radius R centered at p: $N = \{i \in (\text{set of integration points}), i = 1, \ldots, N_p;\ \text{such that}\ \ d_{ip} = ||\mathbf{r}_i - \mathbf{r}_p|| \leq R\}$, where $\mathbf{r}_i$ denotes the position of integration point i. A chosen variable x is averaged at integration point p with the following weighted

average:

$$\overline{x}_p = \frac{\sum_{i=1}^{N_p} x_i\, w_i(d_{ip})}{\sum_{i=1}^{N_p} w_i(d_{ip})} \tag{3}$$

where the weights w_i are defined by the sigmoidal function

$$w_i(d_{ip}) = 2\,\frac{D_{max}^{\gamma}}{D_{max}^{\gamma} + d_{ip}^{\gamma}} - 1 \tag{4}$$

with D_{max} being the radius of the sphere where the average is performed and the constant $\gamma = 2$ was assumed. This function is such that $w_i(0) = 1$ and $w_i(D_{max}) = 0$. Then, D_{max} defines the region where averaging is performed. The model allows the possibility of choosing a different value of D_{max} for each variable to be smoothed, if non-local effects are considered specific for each one. Thus, the radius defining the neighbourhood, R, must be chosen as the maximum of all D_{max}. [1] Here we propose to average the mechanical stimulus at the integration points and provide the state variables as a function of the averaged stimulus (i.e., first perform averaging procedure, then apply Mechanostat model). Another possibility would be simply to average the state variables (i.e., first apply Mechanostat, then perform averaging procedure).

2.4. FE model

The BAM was applied to a simplified model of the diaphysis of the long bone of a small vertebrate. It was built in ABAQUS®[22] and consists in a hollow cylinder of 100 mm in height, 15 mm of outer radius (r_o) and 5 mm of inner radius (r_i), meshed with hexahedral elements. Two types of elements were used: 8-noded hexahedral isoparametric elements, with full integration (8 integration points per element, named C3D8 in ABAQUS element library), and 8-noded hexahedral isoparametric elements, with reduced integration (1 integration point per element, named C3D8R in ABAQUS element library). Two loads were analysed: four-point bending (see Fig. 5, top) such that a bending moment of 100 Nm was applied and torsion (see Fig. 5, bottom) such that a torsion moment of 30 Nm was applied. Three mesh densities were analysed, with 30, 40 and 50 elements spanning the cylinder axis. In the radial and circumferential directions, the number of divisions were such

[1] $D_{max} = R$ if a unique value is used for every variable, as done here.

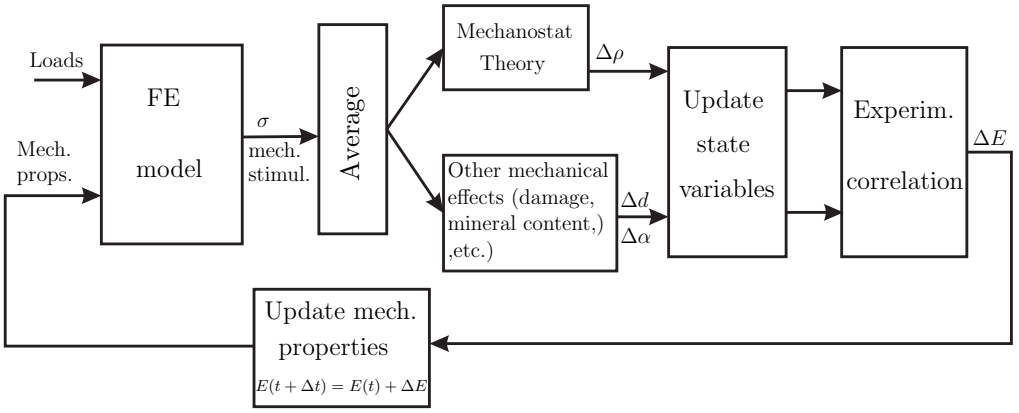

Figure 4: General scheme of a bone adaptation algorithm with control of checkerboard instability through averaging of the mechanical stimulus (either with NBF or NAM).

that elements had an aspect ratio as close to 1 as possible (ranging from 1.2 to 2.1). The total number of elements of each mesh was respectively 1800, 3840 and 8000. In the NAM, three different values of $R = D_{max}$ were used: 3, 4 and 5 mm. The length of the elements and, therefore, the approximate distance between integration points ranges from 0.98 to 4.7 mm. The previous values of R were selected to cover different scenarios, e.g. cases in which just a few neighbouring integration points were inside the sphere of radius R and cases in which many integration points were inside that sphere, in this case without the need for spanning too many elements, which could significantly slow down simulations. The region highlighted in red in Fig. 5 was chosen to show the obtained results. In summary, 2 element types, 2 load cases and 3 meshes were tested, in addition to 3 values of R for NAM.

Finally, a slightly different case was simulated to test the behaviour of the NAM in another situation where checkerboard instability may occur, i.e. problems with stress concentrations or stress singularities. For this purpose, in the cylinder with the finest mesh (50 elements along the cylinder axis) a single element in the middle of the thickness was removed and the bone structure was subjected to uniform compression. For that mesh the dimensions of the void are: height=2mm, inner radius=9 mm, outer radius=11mm, spanned angle=11.25°. This void in the cortical thickness theoretically produces a singular stress field (with stresses tending to infinity), that is captured in the FE model as a stress concentration (increase in the stress level though

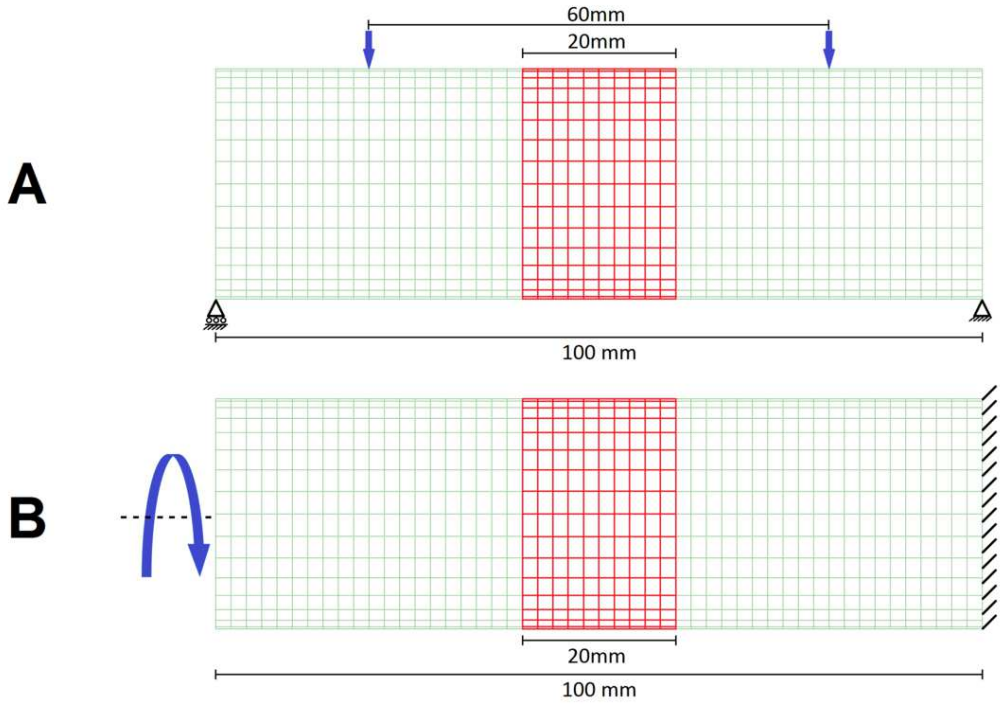

Figure 5: FE models of a beam with cylindrical cross section ($r_i = 5$ mm; $r_o = 15$ mm), with loads and boundary conditions. (A) Four points bending, $M_b = 100$ Nm. (B) Torsion, $M_t = 100$ Nm, applied at the end of the beam with the other end fixed.

not tending to infinity) with an alternating stress pattern in the first two elements next to the void. Such alternating stress pattern may enhance the problem of checkerboard instability.

Simulations were run on a computer with the following characteristics: Intel Core i7-4700MQ processor, 2.4GHz of CPU clock speed, 8Gb RAM memory. With NAM and in the most computationally expensive case (finer mesh, R=5 and full integration), the computing time was 1953s.

2.5. Postprocessing of results

The following variables were defined to evaluate the convergence of the adaptation algorithm, in this case, of the bone volume fraction f_{bm}. First,

an average f_{bm} is evaluated for each step t_i:

$$\overline{f_{bm}}(t_i) = \frac{\int f_{bm}(t_i)\, dV}{\int dV} \times 100 \tag{5}$$

and is expressed in percentage, where the integration is performed over the entire structural domain. If this average tends to a constant value, a global (integral) equilibrium has been reached. An equivalent criterion consists in checking the following average difference, between one step t_i and the next t_{i+1}:

$$\overline{\Delta f_{bm}}(t_{i+1}) = \frac{\int \left(f_{bm}(t_{i+1}) - f_{bm}(t_i)\right) dV}{\int dV} \times 100 \tag{6}$$

also expressed in percentage. This average difference must tend to zero if a global (integral) equilibrium is achieved. However, both criteria establish a necessary though not sufficient condition for convergence. Indeed, those elements that increase their f_{bm} between two consecutive steps (positive difference in Eq. (6)) could compensate those that decrease their f_{bm} (negative difference), such that $\overline{\Delta f_{bm}}$ could tend to zero and $\overline{f_{bm}}$ to a constant value. But this would only indicate the convergence of the integral, that is, the global convergence. Locally, elements could continue to change their f_{bm} throughout the simulation, not ensuring local convergence. This is precisely what occurs in checkerboard situations. For this reason, a necessary and sufficient condition must be defined, for example, through the following average difference:

$$\overline{\overline{\Delta f_{bm}}}(t_{i+1}) = \frac{\int \left|f_{bm}(t_{i+1}) - f_{bm}(t_i)\right| dV}{\int dV} \times 100 \tag{7}$$

again, expressed in percentage. Unless $\overline{\overline{\Delta f_{bm}}}$ tends to zero, a true convergence cannot be ensured. This condition ensures local convergence and thus global convergence. That is, if $\overline{\overline{\Delta f_{bm}}}$ tends to zero, $\overline{f_{bm}}$ tends to a constant value and $\overline{\Delta f_{bm}}$ tends to zero as well. The three criteria were used to show how only the method proposed here achieves local convergence, while the others just reach global convergence, if any, as will be shown in the next section.

3. Results

Bone adaptation simulations started from a uniform bone density distribution, i.e., $f_{bm} = 50\%$. We then applied the respective adaptation algorithm for 50 iteration steps, or until convergence was achieved according to Eqs. (6) and (7) (variation less than 0.005% both in $\overline{\Delta f_{bm}}$ and $\overline{\overline{\Delta f_{bm}}}$), either without control of checkerboard (WCC) or with control procedures, i.e. using NBF and NAM. Note that convergence of $\overline{\overline{\Delta f_{bm}}}$ was always reached later. The final f_{bm} distribution results for these three cases both in bending and torsion are shown for full integration elements (Fig. 6).

It must be noted that, in some cases, the represented range was chosen wider than the meaningful [0,100], in order to facilitate the visualization of the checkerboard instability. The plotted results lie outside the range [0,100] because an extrapolation (without average) is made by default in ABAQUS, from integration points to nodes. So, while f_{bm} is constrained by the BAM to lie within [0,100] at the integration points, the extrapolated value is not.

3.1. Occurrence of checkerboard instability and influence of mesh density

The checkerboard pattern is quite evident in the case WCC, both in bending (close to the neutral axis) and in torsion (at the outer surface). This highlights that checkerboard instability tends to appear in areas of low gradients in f_{bm} (i.e. along the neutral axis in bending or along the circumference in torsion), while steep gradients may hide the checkerboard instability, as it occurs in bending across the direction perpendicular to the neutral axis.

Both smoothing techniques, NBF and NAM, seem to eliminate the checkerboard instability, but some inhomogeneities arise for torsion in NBF at the outer surface. In this case, a homogeneous distribution of f_{bm} in circumferential and axial directions, with a gradient in radial direction, was expected, as it occurs with NAM. Additionally, a different contour range had to be used for NBF and NAM, because the respective f_{bm} values were quite different. In fact, NBF results showed a high dependency on mesh density, which is reflected in Table 2. To illustrate this dependency, Tables 1-3 show the average $\overline{f_{bm}}$ and the convergence parameters ($\overline{\Delta f_{bm}}$, $\overline{\overline{\Delta f_{bm}}}$) at the end of the simulations. It can be seen that, while NAM produced similar values of $\overline{f_{bm}}$ for different mesh densities (see Table 3), this is not the case for WCC and NBF (see Tables 1 and 2). An exception to this is the case NAM with

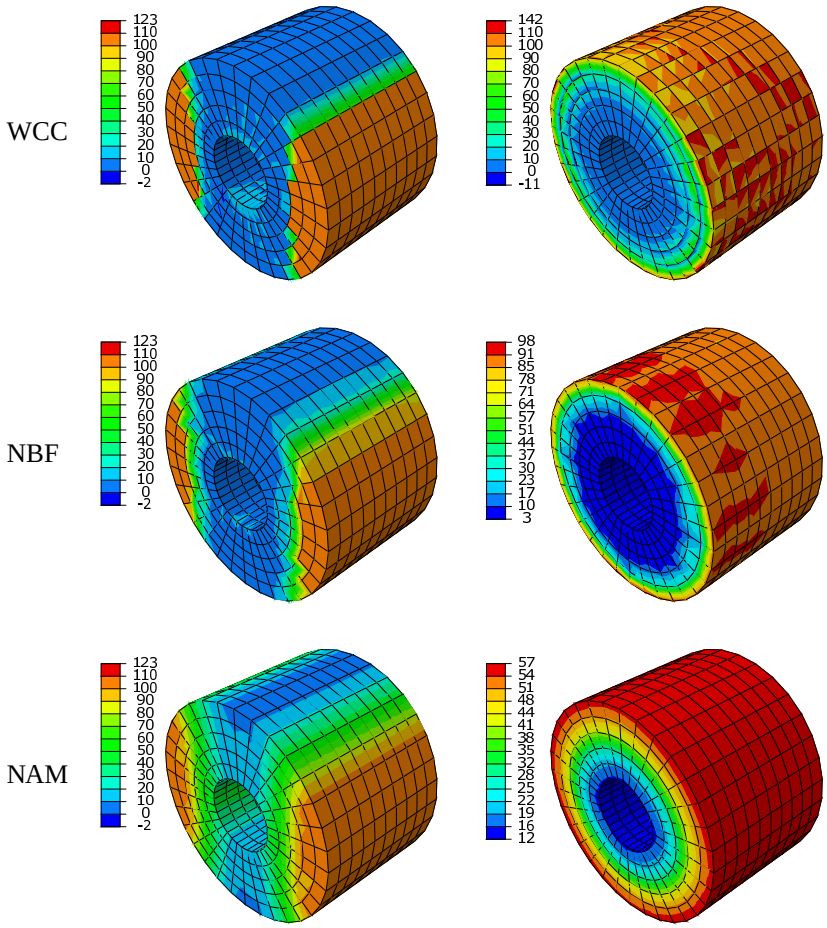

Figure 6: Final distribution of f_{bm} in bending (left) and torsion (right) for full integration elements using the finest mesh (50 divisions along the cylinder axis) together with application of WCC (top panel), NBF (middle panel) and NAM with $R = 4$ mm (bottom panel). WCC: without control of checkerboard, NBF: node-based formulation, NAM: neighbourhood averaging method.

$R = 3$mm, because this radius is too small to perform a proper average, as will be discussed later.

3.2. Full vs. reduced integration

Fig. 7 shows the final distribution of f_{bm} for simulations with reduced integration elements. In contrast to Fig. 6, f_{bm} lies within [0,100] because these elements only contain one integration point and no extrapolation is made inside them. Thus, f_{bm} is constant within the element and constrained to lie in the range [0,100]. With reduced integration, checkerboard instability is more evident in bending for the case WCC (see top panel Fig. 7), as opposed to full integration, when it was more pronounced in torsion. It can also be noted that the solutions obtained with NBF and NAM are very similar for reduced integration.

Comparison of $\overline{f_{bm}}$ obtained for full and reduced integration elements (see Tables 1-3) showed another interesting result: the solutions obtained with WCC and NBF are very sensitive to the type of integration, while those obtained with NAM are not. The reason may be that reduced integration is an average itself, because the state variable at the single integration point represents an average in the whole element and NAM performs an average in a domain that is similar to one element, at least if R is properly chosen.

3.3. Proper selection of R in NAM

This observation opens the discussion on the proper choice of R in NAM. Fig. 8 shows the solutions obtained for two different values of R and compares them with WCC for torsion. If R is chosen too small, not enough integration points are inside the neighbourhood and the average could be very poor or even non-existent, as it occurs for $R = 0.5$mm, which leads to the same solution obtained with WCC. On the other hand, an excessively large R could hide gradients and distort the solution in certain cases. Consequently, R must be chosen very carefully and accordingly with the mesh density.

3.4. Analysis of convergence

Another important aspect to be analysed is the convergence of simulations. As stated before, convergence was assumed if the following conditions hold: $\overline{\Delta f_{bm}} < 0.005\%$ and $\overline{\overline{\Delta f_{bm}}} < 0.005\%$. If convergence was not achieved after 50 steps, the simulation was stopped. The obtained values for the different algorithms are summarised in Tables 1-3 along with the step when convergence was achieved (or 50 if the simulation had to be stopped). In

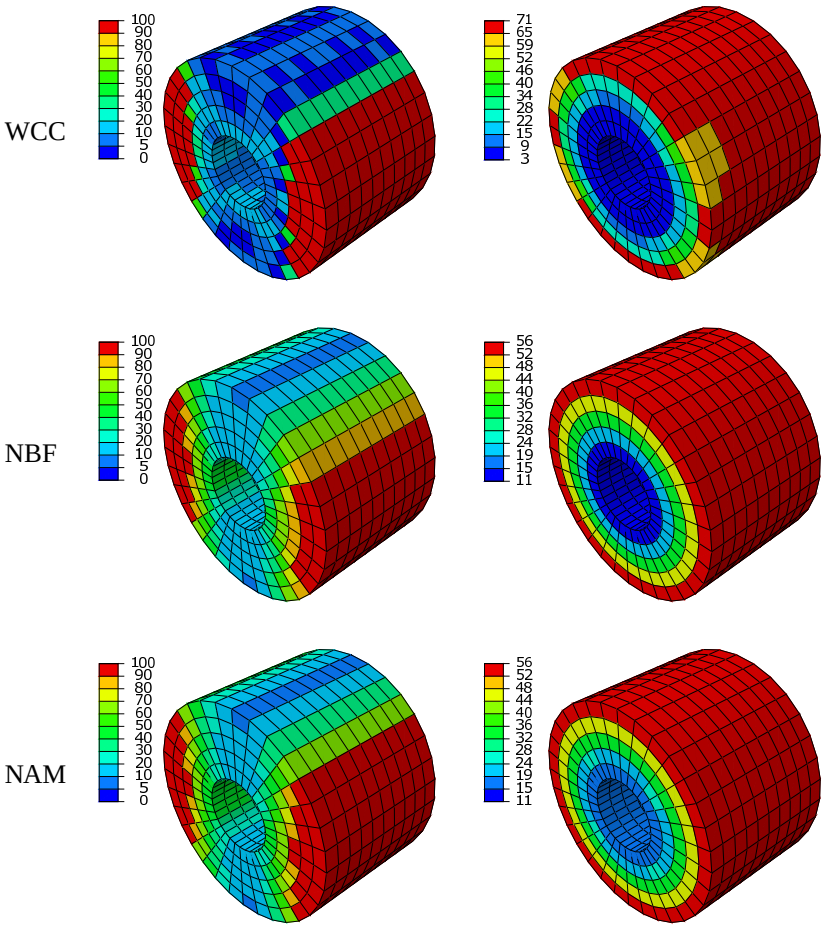

Figure 7: Final distribution of f_{bm} in bending (left) and torsion (right) for reduced integration elements using the finest mesh (50 divisions along the cylinder axis) together with application of WCC (top panel), NBF (middle panel) and NAM with $R = 4$ mm (bottom panel). WCC: without control of checkerboard, NBF: node-based formulation, NAM: neighbourhood averaging method.

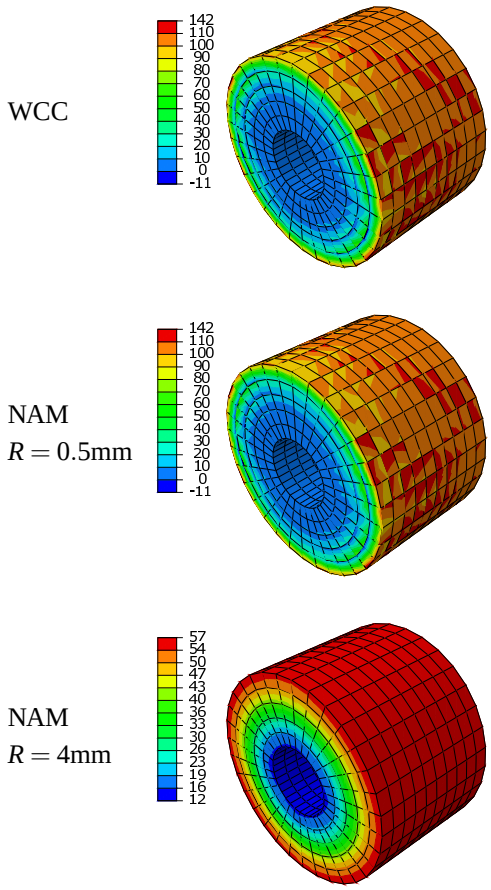

Figure 8: Comparison of the distribution of f_{bm} obtained with WCC and NAM for 2 different values of R, in torsion, for full integration elements and the finest mesh. WCC: without control of checkerboard, NAM: neighbourhood averaging method.

Load	Integration	Mesh	$\overline{f_{bm}}(\%)$	$\overline{\Delta f_{bm}}(\%)$	$\overline{\overline{\Delta f_{bm}}}(\%)$	step
Bending	Full	30	47.185	-0.1090	0.1687	50
		40	46.952	-0.1287	0.1911	50
		50	46.918	-0.1159	0.1804	50
	Reduced	30	54.202	-0.0180	0.0467	50
		40	52.390	-0.0337	0.0787	50
		50	50.823	-0.0357	0.0866	50
Torsion	Full	30	24.326	-0.1303	0.1819	50
		40	23.746	-0.1728	0.2430	50
		50	23.563	-0.1906	0.2737	50
	Reduced	30	31.404	-0.0085	0.0391	50
		40	28.732	-0.0704	0.1239	50
		50	27.466	-0.0751	0.1539	50

Table 1: Summary of results for simulations without control of checkerboard (WCC).

addition, Fig. 9 shows the evolution of the average $\overline{f_{bm}}$ for the three different algorithms as a function of iteration step. It can be observed that NAM produced a stable solution, which was almost independent of mesh density. On the contrary, WCC did not achieve convergence within 50 steps. NBF provided solutions that highly depended on mesh density. Noticeable oscillations occurred between steps 10 and 20, but convergence was finally reached after these oscillations were attenuated (Fig. 9). Fig. 10 supports the notion of convergence and, although some smaller oscillations can still be seen at the end of the simulations, $\overline{\Delta f_{bm}} < 0.005\%$ was achieved for all algorithms. However, these results are not conclusive and it must be acknowledged that the solution did not converge with NBF, due to the fact that $\overline{\overline{\Delta f_{bm}}}$ did not tend to zero (see Fig. 11). This indicates that some fluctuations of f_{bm} must have occured in certain elements, but they were compensating each other, such that $\overline{f_{bm}}$ seemed to tend to a stable value, but with alternating values of f_{bm} in certain regions. In other words, the checkerboard pattern was not fully corrected with NBF. On the contrary, NAM reached convergence very quickly (roughly after 15 steps), as can be seen in Fig. 11. WCC cases tended to convergence, though very slowly and not within 50 iteration steps. Furthermore, it must be emphasised that WCC solutions exhibited a checkerboard pattern though convergence might have occurred.

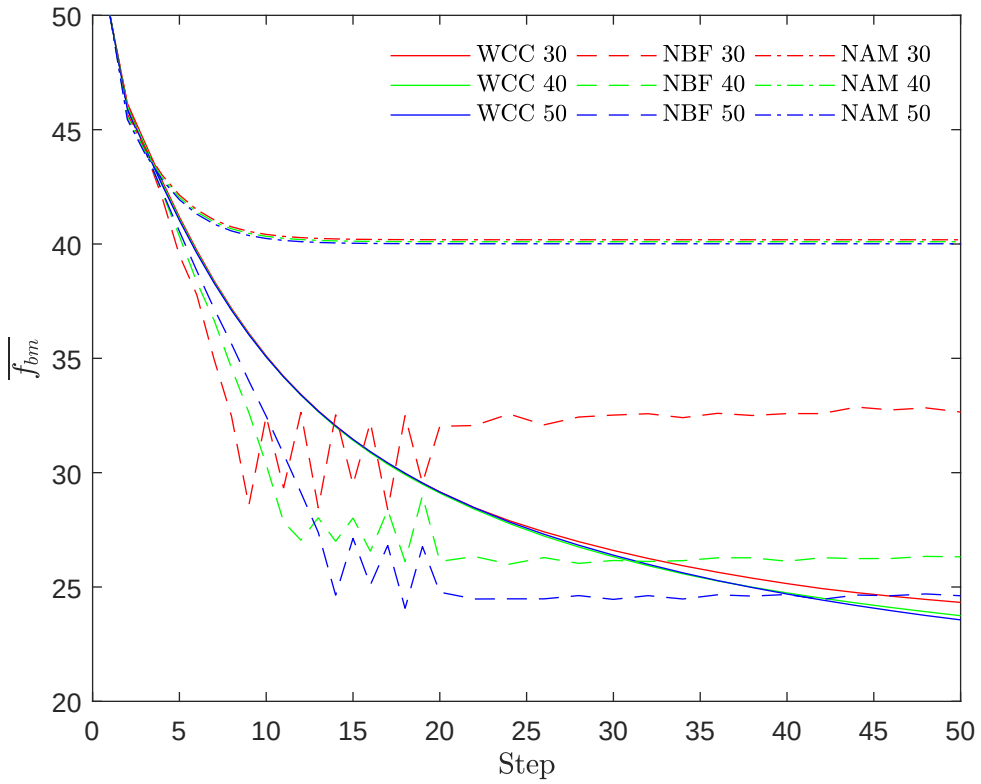

Figure 9: Evolution of $\overline{f_{bm}}$ through the simulation for WCC, NBF and NAM ($R = 4$ mm), in torsion, full integration elements and different mesh densities (30, 40 and 50 elements along the cylinder axis). WCC: without control of checkerboard, NBF: node-based formulation, NAM: neighbourhood averaging method.

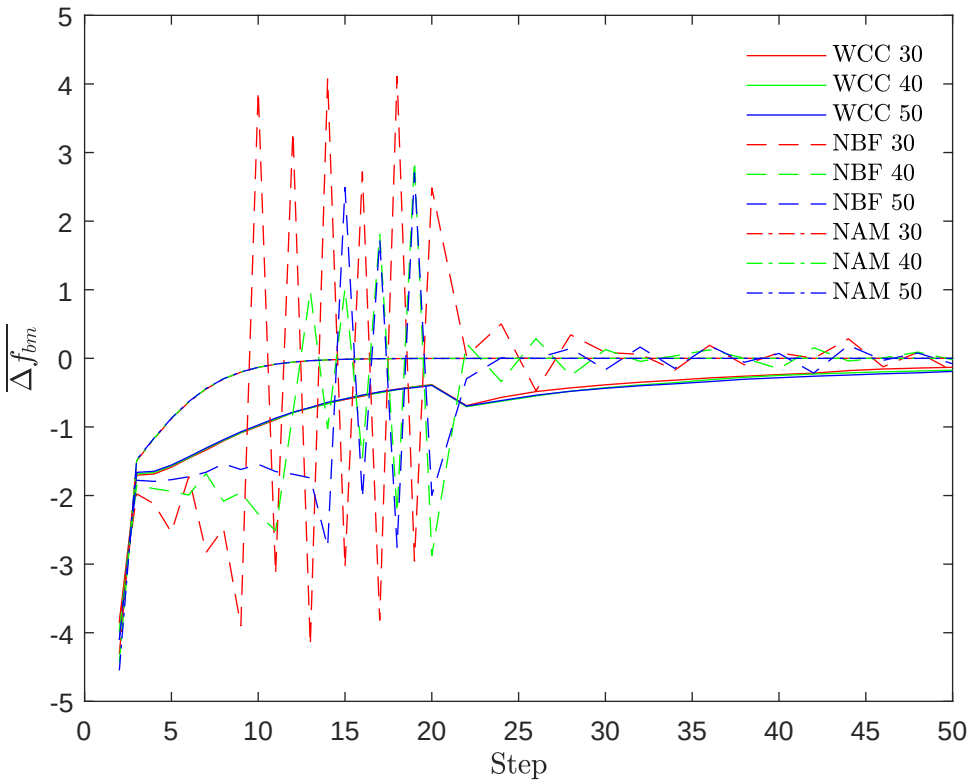

Figure 10: Evolution of $\overline{\Delta f_{bm}}$ through the simulation for WCC, NBF and NAM ($R = 4$ mm), in torsion, full integration elements and different mesh densities (30, 40 and 50 elements along the cylinder axis). WCC: without control of checkerboard, NBF: node-based formulation, NAM: neighbourhood averaging method.

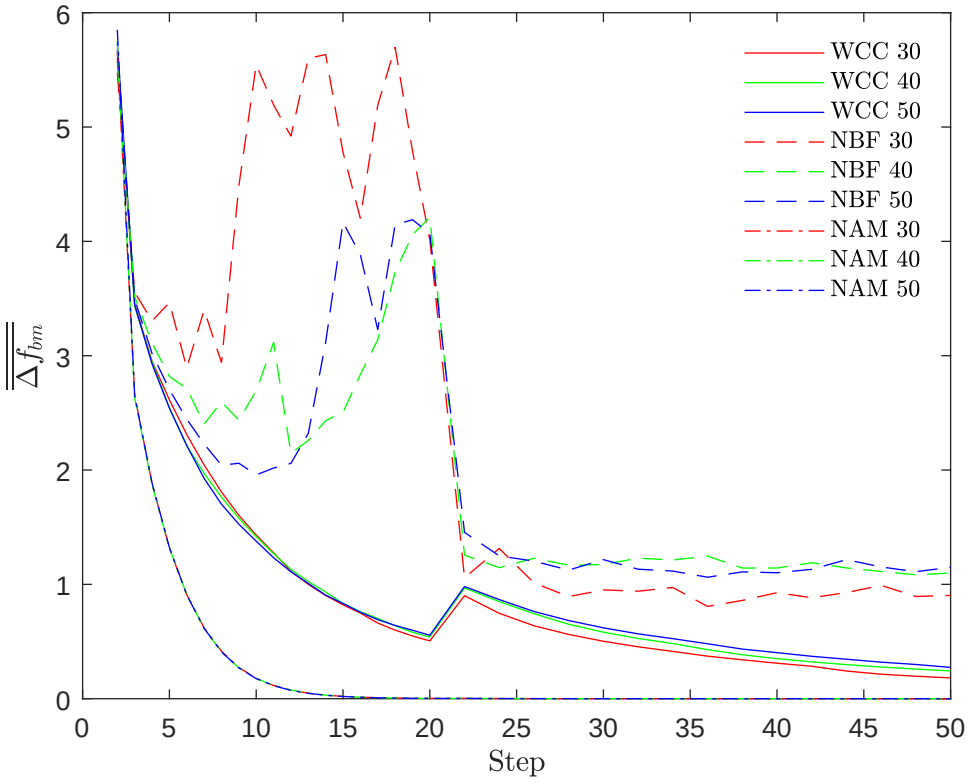

Figure 11: Evolution of $\overline{\overline{\Delta f_{bm}}}$ through the simulation for WCC, NBF and NAM ($R = 4$ mm), in torsion, full integration elements and different mesh densities (30, 40 and 50 elements along the cylinder axis). WCC: without control of checkerboard, NBF: node-based formulation, NAM: neighbourhood averaging method.

Load	Integration	Mesh	$\overline{f_{bm}}(\%)$	$\overline{\Delta f_{bm}}(\%)$	$\overline{\overline{\Delta f_{bm}}}(\%)$	step
Bending	Full	30	47.996	-0.2311	0.6833	50
		40	46.710	-0.0360	0.6663	50
		50	44.843	-0.0537	0.8575	50
	Reduced	30	65.890	-0.0021	0.0038	15
		40	63.290	-0.0026	0.0042	17
		50	60.887	-0.0025	0.0040	20
Torsion	Full	30	32.651	-0.1828	0.9033	50
		40	26.319	-0.0198	1.0993	50
		50	24.618	-0.0794	1.1498	50
	Reduced	30	42.461	-0.0029	0.0040	16
		40	40.718	-0.0029	0.0039	20
		50	39.265	-0.0025	0.0032	26

Table 2: Summary of results for simulations with node-based formulation (NBF).

3.5. Stress singularities

A different situation is analysed in the following, i.e. inducing a void/hole in the domain which produces a stress concentration. The cylinder was subjected to uniform compressive loading. Notably, if the void has sharp corners, as it is the case when a single element is removed, the analytical solution will yield a stress singularity at the corners of the void, with stresses tending to infinity. A similar scenario may be observed for FE simulations of titanium implants inserted into bone. FE models cannot reproduce these singular solutions with infinite stresses unless special elements (such as quarter-point elements) or enhanced methods (such as the generalized finite element method) are used. With the standard formulation and using standard elements, a spurious solution with oscillating stress patterns is obtained in theses cases. Such stress pattern is very noticeable in the first two elements next to the singularity, i.e. the void or bone-implant interface [23, 24]. This type of problem increases the chance of checkerboard pattern to occur (see Fig. 12). In this case, reduced integration was used to show the effect more clearly, though similar results are obtained using full integration.

Stress oscillations were present in all cases, giving rise to spatial oscillations of f_{bm}, but they were more pronounced using WCC, as it can be easily noticed in the circumferential direction in Fig. 12, where an alternating colour pattern (green-yellow-green) appears. When a smoothing technique

Load	Integration	Mesh	R	$\overline{f_{bm}}(\%)$	$\overline{\Delta f_{bm}}(\%)$	$\overline{\overline{\Delta f_{bm}}}(\%)$	step
Bending	Full	30	3	59.459	-0.0019	0.0050	26
			4	62.230	-0.0017	0.0040	18
			5	64.418	-0.0011	0.0031	16
		40	3	59.685	-0.0010	0.0039	28
			4	62.172	-0.0011	0.0037	19
			5	64.264	-0.0009	0.0030	16
		50	3	59.654	-0.0013	0.0038	26
			4	62.117	-0.0015	0.0039	18
			5	64.102	-0.0010	0.0030	16
	Reduced	30	3	54.266	-0.0174	0.0458	50
			4	61.307	-0.0015	0.0043	42
			5	64.929	-0.0008	0.0043	18
		40	3	58.060	-0.0030	0.0044	40
			4	62.325	-0.0017	0.0038	20
			5	64.883	-0.0011	0.0032	15
		50	3	59.691	-0.0013	0.0035	28
			4	62.574	-0.0018	0.0042	17
			5	64.290	-0.0018	0.0047	15
Torsion	Full	30	3	38.334	0.0000	0.0043	32
			4	40.189	-0.0021	0.0039	19
			5	41.191	-0.0028	0.0042	16
		40	3	38.523	-0.0003	0.0037	28
			4	40.103	-0.0021	0.0037	19
			5	41.085	-0.0031	0.0045	16
		50	3	38.447	-0.0004	0.0034	28
			4	40.014	-0.0020	0.0035	19
			5	40.999	-0.0027	0.0041	16
	Reduced	30	3	31.356	-0.0096	0.0320	50
			4	40.268	-0.0010	0.0047	24
			5	41.417	-0.0023	0.0036	17
		40	3	38.761	0.0000	0.0046	32
			4	40.472	-0.0017	0.0036	19
			5	41.263	-0.0028	0.0039	16
		50	3	38.675	0.0000	0.0045	28
			4	40.153	-0.0030	0.0046	18
			5	41.131	-0.0030	0.0043	16

Table 3: Summary of results for simulations with neighbourhood averaging method (NAM).

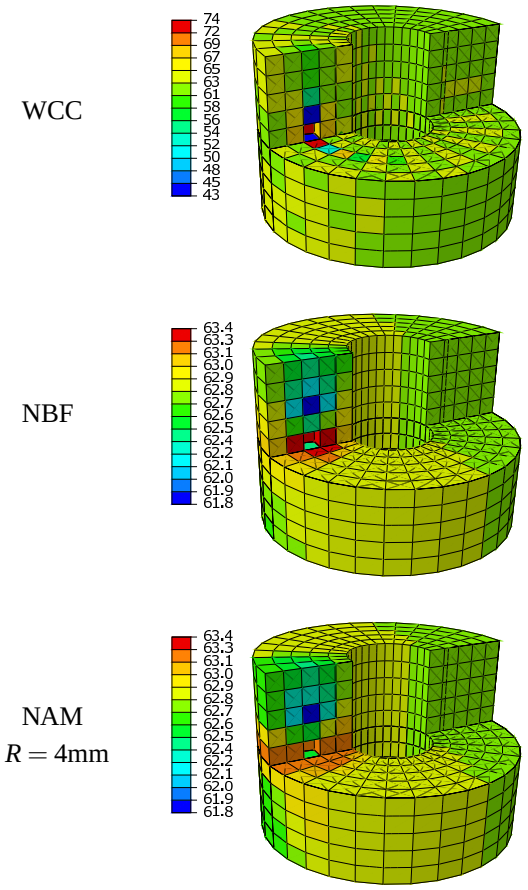

Figure 12: Final distribution of f_{bm} under uniform compression in a model with a void in the middle of the cortex, for WCC, NBF and NAM ($R = 4$mm), with reduced integration elements and the finest mesh (50 elements along the cylinder axis). WCC: without control of checkerboard, NBF: node-based formulation, NAM: neighbourhood averaging method.

was used, these oscillations were not so strong and the contour range had to be adjusted (i.e. reduced) for visual presentation. Moreover, f_{bm} was homogeneous sufficiently far from the stress concentration, except for WCC where the instability produced by the void spread all over the model and the checkerboard pattern could be easily observed. Both the NBF and NAM, performed well to correct the checkerboard pattern far from the void and were able to reduce it in its vicinity. However, NBF still exhibited the above mentioned problems: an excessive influence of mesh density and a lack of convergence to a stable solution.

4. Discussion

Checkerboard patterns arise in bone adaptation simulations due to the governing adaptation equations (i.e., the Mechanostat Theory/Wolff's law) which introduces a positive feedback between bone apparent density and the applied load: density increases with load making bone stiffer, which makes it attract more load. For this reason, an eventual perturbation of density in a region where uniform density is expected, for example due to numerical issues, may become unstable as discussed in the two-unit model (Fig. 2). This unstable behaviour has two potential consequences: the patchwork pattern usually found in the density distribution and the lack of convergence, as density may oscillate locally.

Our numerical simulations indicated that a checkerboard pattern was more evident in regions where density was approximately uniform, while steep gradients in density may mask the phenomenon to some extent. This is the reason why the checkerboard pattern was more noticeable in torsion along circumferential and axial directions and in bending close to the neutral axis.

Smoothing techniques were useful to eliminate checkerboard instability and both NBF and NAM performed well in this regard. However, NBF exhibited certain weaknesses that are discussed below.

4.1. Full vs. reduced integration

The use of full versus reduced integration affected the results significantly. Without smoothing (WCC), the checkerboard pattern seemed more evident for torsion with full integration and for bending with reduced integration, but it must be acknowledged that it was present in all cases and it was just the choice of the contour range what made it more evident in one case or another.

But the type of integration did affect the results more notably when smoothing/averaging techniques were used. NBF performed worse than NAM with full integration, but, as could be expected, the solutions obtained with NBF and NAM were very similar for reduced integration (see Fig. 7). Indeed, the main difference between both procedures is that NBF extrapolates state variables from the integration points to the nodes and averages the extrapolated values at the nodes, while NAM only performs an average of raw (non-extrapolated) values. Since no extrapolation is possible in reduced integration elements, both procedures are similar in this case and so are the obtained solutions. This similarity between NBF and NAM for reduced integration suggests that the extrapolation performed in NBF may be partly responsible for the poor performance of the method with full integration.

The remaining differences between NBF and NAM are: 1) the point where the average is made (nodes in NBF and integration points in NAM), 2) the region within which the average is made (the patch associated to the node in NBF and the neighbourhood N in NAM) and 3) the type of average (regular in NBF and weighted in NAM). These are subtle differences and would explain the little variations found between NBF and NAM for reduced integration elements.

4.2. Influence of mesh density

Another feature that might influence the performance of the smoothing technique is mesh density. Prior to checking the convergence of NAM and NBF, the convergence of the FE method (invariance of the solution with the number of degrees of freedom) must be analysed first, by comparing the solutions of WCC for the three mesh densities. Since WCC produced similar results for the three models, convergence of the FE method can be assumed. However, the convergence of the other simulations was very different from each other. As opposed to NAM, which produced identical results for the three mesh densities, NBF was very sensitive to the element size (see Fig. 9 and Table 2), and particularly in torsion with full integration, where the gradient of f_{bm} was particularly pronounced in radial direction. Again, the extrapolation performed in NBF seems to be the reason for its bad performance, because it is in cases with steep gradients when that extrapolation is more prone to numerical issues.

The convergence of bone adaptation simulations needs to be assessed through $\overline{\overline{\Delta f_{bm}}}$, which is able to detect local changes in f_{bm} by calculating the absolute difference between successive estimations. If just the difference is

accounted for (as in $\overline{\Delta f_{bm}}$) or if the simple stabilisation of the average $\overline{f_{bm}}$ is used, only the global convergence can be detected. Fluctuations of f_{bm} at a local scale, that are typical of checkerboard instability, might remain undetected by $\overline{\Delta f_{bm}}$ or might not produce a significant change in $\overline{f_{bm}}$, because those fluctuations could compensate for one another. In such case, the solution cannot be assumed as converged. This is exactly what occurred to NBF simulations, which seemed to have converged in light of $\overline{f_{bm}}$ and $\overline{\Delta f_{bm}}$, though $\overline{\overline{\Delta f_{bm}}}$ showed they had not. In other words, NBF did not achieve convergence for the bone adaptation scenarios simulated here.

4.3. Proper selection of R in NAM

In all simulations, NAM performed very robustly and much better than NBF. It provided solutions that were almost independent of mesh density and type of integration (see Table 3) and convergence was achieved very quickly. However, the choice of R is of the most importance, as Fig. 8 proved. If the chosen R is too small, no meaningful average can be performed and the solutions are identical to those obtained without control of checkerboard (WCC). The value $R = 0.5$ mm was chosen too small on purpose, in order to illustrate that idea, but even $R = 3$ mm seemed inappropriate because it produced solutions that differed from those obtained with $R = 4$ mm and $R = 5$ mm, which were more similar to each other (see Table 3).

If R is too large, the computational cost increases because more integration points enter the neighbourhood and must be accounted for in the calculations. Besides, an excessively large R (or D_{max})[2] could hide gradients and alter a specific solution making it unnecessarily uniform. To avoid this, the average was weighted with the distance to the centre of the neighbourhood, being the parameter γ essential to control the influence of distant points. So, D_{max} and γ must be chosen accordingly to the type of problem, the mesh density and the variable to be averaged. For example, in the BAM used here [25] some biochemical factors influence on bone response and two of them have a totally different way to act in the system. RANKL is a molecule expressed on the surface of osteoblasts and, thus, its concentration is linked to the presence of those cells. OPG is a soluble protein which is also produced by osteoblasts, but it does not remain bound to their surface. For this

[2]Recall that R is the size of the neighbourhood and D_{max} is the distance up to which the average is performed.

reason, it is plausible to think that diffusion of RANKL be more constrained than that of OPG and, consequently, its radius of influence should be shorter. In this case, a smaller value of D_{max} could be chosen for RANKL.

The former idea of attenuation of biochemical signals is in the background of some BAMs, such as those developed by Huiskes and co-workers [17, 26]. In these models, bone response depends on strain energy density and mechanosensitivity of osteocytes (their ability to sense that strain energy density), which stimulate osteocytes to produce a biochemical messenger. This biochemical messenger causes signals to be dissipated through the osteocytic network towards the bone surface, where they create an osteoblast recruitment stimulus [27], and the attenuation of those signals with distance is accounted for through an exponential decay function [26], which is analogous to the average proposed here.

It is also important to note that special care must be taken when selecting R in geometries with non-convex domains, to avoid non-physical situations such as the smoothing algorithm acting across the inner radius of the cylinder. To take this into account R could be reduced close to non-convex bounds.

4.4. Purposely discontinuous solutions

Weinans et al. [15] argued that the patchwork distribution of density represented the discontinuous solution of a problem which, in the case of trabecular bone, was closer to reality than the continuous (smoothed) solution, as trabeculae make up a discontinuous structure. In such case, checkerboard instability could be beneficial to the purpose of modelling bone, but it must not be forgotten that the solution, and particularly the size of the discontinuity, would depend on mesh density as discussed before and, more importantly, it would not be controlled by biological factors, but by mathematical ones. This would force using an element size in accordance with trabecular size, which vary across regions, and it could make it difficult to build the FE model. The NAM algorithm presents an alternative to obtain purposely discontinuous solutions, by choosing an adequate D_{max}. This strategy could be meaningful from a biological point of view, if D_{max} is chosen based on physiological aspects, and can be very easily implemented and modified without the need of changing the mesh. Notwithstanding, the mesh should always be fine enough to approximate the problem in its true scale. Recalling the BAMs by Huiskes and co-workers, the osteocytic signal is completely attenuated at distances in the order of microns, a much shorter scale than the typical D_{max} used here. To implement the attenuation of osteocytic signals

with the present model, D_{max} should be reduced and the FE mesh refined accordingly, so as to have elements smaller than the neighbourhoods; otherwise, no average would be performed. In other words, D_{max} and the mesh size must be adapted to the scale of the specific problem and to size of the allowed (or sought) discontinuities.

4.5. Solutions with singularities

The solution of the elastic problem gives rise to a singular stress field under certain circumstances and at certain points, for example a re-entrant corner or a two-material wedge [28], a situation which is typical of implants. Unless special elements or enhanced methods are used, stress singularities cannot be captured in FE simulations, which instead reproduce a stress concentration, eventually leading to checkerboard instability. We have proven that our smoothing algorithm can mitigate this problem to some extent, though it cannot eliminate the discontinuity of stresses in the elements adjacent to the singularity, which is inherent to this particular FE solution.

The singularity only appears at the corner for certain angles of the concurrent wedges, generally in a re-entrant corner of 90° or less. Although this situation can be found in a FE model, let us think of an implant perpendicular to the bone surface, it is improbable to find re-entrant corners in real situations, because bone is likely resorbed due to stress shielding [24], thus smoothing the corner. This is what occurs, for example, in crestal bone loss around dental implants [29]. A smoothing technique such as the one proposed here can help to avoid these unrealistic situations by defining a large value of D_{max} around the implant that is sufficient to mask spurious stress singularities. In other words, NAM has the ability to disregard excessively local effects that may arise exclusively from the mesh and not from the underlying biology.

5. Summary and conclusions

Checkerboard instability is typically found in bone adaptation simulations and can significantly compromise the convergence of results and the reliability of FE simulations. Here we have a proposed a new method to address this algorithmic issue using on a non-local smoothing technique. While different smoothing techniques have also been proposed by other authors, the current method exhibited the following advantages over previous ones:

- No influence of the type of integration was observed with NAM, in contrast to NBF which performed very poorly for full integration.
- NBF was very sensitive to mesh density, likely due to the extrapolation performed from integration points to nodes. NAM overcame these difficulties and yielded solutions that were independent of the mesh density, provided that the mesh density was sufficiently large to ensure convergence of the FE method.
- Convergence of bone adaptation simulations was only ensured with NAM. NBF produced oscillations of bone volume fraction through the simulation and only achieved a poor convergence of bone volume fraction at a global level, but not locally. Another advantage of NAM was an improved convergence rate.
- The choice of D_{max} and γ can provide control over how localised a specific biological process is accounted for.

We believe that this new algorithm for bone adaptation simulations, which is provided in "Supplementary Materials", will help address a variety of problems in bone biology and orthopaedics.

6. Acknowledgements

Funding was provided by the *Consejería de Economía, Conocimiento, Empresas y Universidad, Junta de Andalucía* through the research project P18-RT-3611 entitled *Efecto combinado del ejercicio físico y el denosumab en el tratamiento de la osteoporosis. Diseño de un tratamiento farmacológico específico de paciente* for which this paper has been prepared.

7. References

[1] Campo M, Fernández J, Kuttler K, Shillor M. Quasistatic evolution of damage in an elastic body: numerical analysis and computational experiments. Appl Numer Math 2007;57(9):975–88.

[2] Li J. A micromechanics-based strain gradient damage model for fracture prediction of brittle materials – part i: Homogenization methodology and constitutive relations. Int J Solids Struc 2011;48(24):3336–45.

[3] Sigmund O, Petersson J. Numerical instabilities in topology optimization: a survey on procedures dealing with checkerboards, mesh-dependencies and local minima. Struct Optimization 1998;16(1):68–75.

[4] Matsui K, Terada K. Continuous approximation of material distribution for topology optimization. Int J Numer Met Eng 2004;59(14):1925–44.

[5] Doblaré M, García J. Anisotropic bone remodelling model based on a continuum damage-repair theory. J Biomech 2002;35(1):1–17.

[6] Fernández J, García-Aznar JM, Martínez R. Numerical analysis of a diffusive strain-adaptive bone remodelling theory. Int J Solids Struc 2012;49(15-16):2085–93.

[7] Chambon R, Caillerie D, Matsuchima T. Plastic continuum with microstructure, local second gradient theories for geomaterials: localization studies. Int J Solids Struc 2001;38(46-47):8503–27.

[8] Lorentz E, Godard V. Gradient damage models: Toward full-scale computations. Comput Methods Appl Mech Eng 2011;200(21-22):1927–44.

[9] Fyhrie D, Carter D. A unifying principle relating stress to trabecular bone morphology. J Orthop Res 1996;4:304–17.

[10] Fernandes P, Rodrigues H, Jacobs C. A model of bone adaptation using a global optimisation criterion based on the trajectorial theory of wolff. Comput Methods Biomech Biomed Engin 1999;2(2):125–38.

[11] Jacobs C, Levenston M, Beaupré G, Simo J, Carter D. Numerical instabilities in bone remodeling simulations: the advantages of a node-based finite element approach. J Biomech 1995;28(4):449–59.

[12] Frost H. Bone's mechanostat: A 2003 update. The Anatomical Record Part A 2003;275(A):1081–101.

[13] Reina J, García-Aznar J, Domínguez J, Doblaré M. Numerical estimation of bone density and elastic constants distribution in a human mandible. J Biomech 2007;40(4):828–36.

[14] Garijo N, Fernández J, Pérez M, García-Aznar J. Numerical stability and convergence analysis of bone remodeling model. Comput Method Appl M 2014;271:253–68.

[15] Weinans H, Huiskes R, Grootenboer H. The behavior of adaptive bone-remodeling simulation models. J Biomech 1992;25(12):1425–41.

[16] Chen G, Pellet G, Pearcy M, McElwain D. Comparison of two numerical approaches for bone remdelling. Med Eng Phys 2007;29:134–9.

[17] Huiskes R, Ruimerman R, van Lenthe H, Janssen J. Effects of mechanical forces on maintenance and adaptation of form in trabecular bone. Nature 2000;8:704–6.

[18] Hernandez C, Beaupré G, T.S. K, Carter D. The influence of bone volume fraction and ash fraction on bone strength and modulus. Bone 2001;29(1):74–8.

[19] Martínez-Reina J, García-Aznar J, Domínguez J, Doblaré M. On the role of bone damage in calcium homeostasis. J Ther Biol 2008;254(3):704–12.

[20] Lemaitre J, J.L. C. Mechanics of Solid Materials. Cambridge, UK: Cambridge University Press; 1990.

[21] García-Aznar J. A bone remodelling model coupling microdamage growth and repair by 3d bmu-activity. Biomech Model Mechanobiol 2005;4(2-3):147–67.

[22] Dassault Systems. Simulia. ABAQUS UNIFIED FEA; Accessed: 2020-09-10. https://www.3ds.com/products-services/simulia/products/abaqus.

[23] Ojeda J, Martínez-Reina J, García-Aznar J, Domínguez J, Doblaré M. Numerical simulation of bone remodelling around dental implants. P I Mech Eng H 2011;225(9):897–906. doi:10.1177/0954411911410165.

[24] Martínez-Reina J. Aplicación de modelos de remodelación ósea interna al estudio del comportamiento de implantes dentales. Ph.D. thesis; Universidad de Sevilla; 2006.

[25] Martínez-Reina J, Pivonka P. Effects of long-term treatment of denosumab on bone mineral density: insights from an in-silico model of bone mineralization. Bone 2019;125(125):87–95. URL: https://www.ncbi.nlm.nih.gov/pubmed/31055117. doi:10.1016/j.bone.2019.04.022.

[26] Ruimerman R, Hilbers P, van Rietbergen B, Huiskes R. A theoretical framework for strain-related trabecular bone maintenance and adaptation. J Biomech 2005;38:931–41.

[27] Burger E, Klein-Nulend J. Mechanotransduction in bone–role of the lacuno-canalicular network. FASEB J 1999;13:S101–12.

[28] Hein V, Erdogan F. Stress singularities in a two-material wedge. Int J Fract Mech 1971;7:317–30.

[29] Albrektsson T, Buser D, Sennerby L. Crestal bone loss and oral implants. Clin Implant Dent R 2012;14(6):783–91.

Appendix

Bone adaptation model

In this paper we have used the BRM developed by Martínez-Reina and Pivonka [25] to build a phenomenological BRM. This model provides bone cell populations for a given stress level and mechanobiological environment. Based on these populations, changes of bone volume fraction (f_{bm}) can be obtained along with variation of mineral content (α), which was assessed through an algorithm implementing the bone mineralization process. We also used the damage model proposed in [19] to estimate microstructural damage (d).

For a given uniaxial stress we simulated a homeostatic situation using the BRM until a bone adaptation equilibrium was reached. Next, the uniaxial stress was varied within a physiological range to get the curves of f_{bm}, d and α shown in Fig. 13 and distinguishing between tension and compression.

Those curves were then used to propose an indirect phenomenological BRM. First, the principal stresses ($\sigma_1 > \sigma_2 > \sigma_3$) were obtained from the FE model at every point. The absolute values of the maximum and minimum principal stresses were compared to choose between tension and compression curves. The maximum of those two values was used as the mechanical stimulus driving bone adaptation:

$$\sigma_{max} = max(|\sigma_1|, |\sigma_3|) \tag{8}$$

Following, σ_{max} was used in Figs. 13 to obtain the state variables: f_{bm}, d and α. Finally, Eq. 2 was used to provide the new Young's modulus at every

point. Since stresses could be redistributed by the change of Young's modulus, this process had to be repeated until the distribution of state variables remained constant. In the case of using an smoothing/averaging technique, every stress component was smoothed, either at the nodes (in the NBF) or at the integration points (in the NAM). Next, the resulting stress tensor was used to evaluate the mechanical stimulus, σ_{max}, using Eq. 8, and this was used in Figs. 13 to obtain the state variables, which, as a consequence, resulted smoothed and continuous. This indirect phenomenological BRM was chosen to save computing time and is justified by the fact that the performance of the smoothing technique is independent of the BRM, as could be checked by implementing it with different BRMs.

Brief description of the code

The routine *NAM.for* used to implement the NAM is briefly explained in this section and provided as Supplementary Material. A flowchart of the code is shown in Fig. 14. The routine is divided in the following steps:

1. **Read tables $f_{bm} - \alpha - d$ vs. stress**

   Data in Fig. 13 are given as tables in files *tcomp.txt* and *ttens.txt*, which relate stress to f_{bm}, α and d, for compression and tension, respectively. These tables are stored as global variables (in ABAQUS, it is made using the subroutine named *UEXTERNALDB*, with variable $LOP = 0$, which means that the execution of this part of the code is performed at the beginning of the analysis).

2. **Collection of global coordinates of integration points**

   Global coordinates of integration points are stored in the global variable *COORDS2* (in ABAQUS, these coordinates are available in subroutine named *SDVINI*, which is called right after *UEXTERNALDB* $LOP = 0$).

3. **Definition of the neighbourhood corresponding to every integration point**

   For a given integration point p and a given radius R, the neighbourhood is defined by those integration points within the sphere of radius R and centred at p. The identification of these points is made in subroutine *NEIGHBORHOOD2*, based on the coordinates collected in step

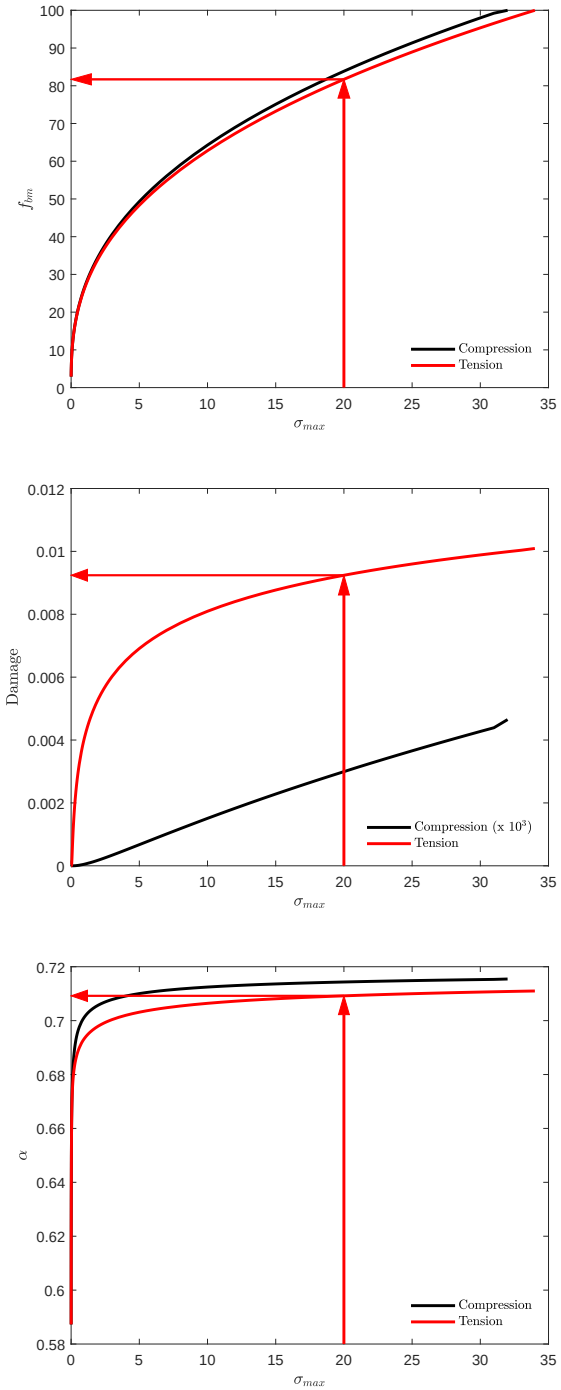

Figure 13: Curves that provide the values of f_{bm}, d and α obtained with the BRM proposed in [25] for a homeostatic situation and a given value of uniaxial stress.

2 and the global variable *NEIGHB* is stored with the information of the neighbourhoods. Two substeps are performed at this stage:

3.1. First, in subroutine *NEIGHBOURHOOD1*, the maximum number of neighbour integration points contained in any neighbourhood is calculated. This is needed to dimension the variable *NEIGHB* correctly. This substep is only needed the first time a model is run. For subsequent analyses, the dimension of *NEIGHB* is known and memory can be easily allocated, so that this part of the code can be commented.

3.2. Once memory is correctly allocated, the information of neighbourhoods is stored in *NEIGHB* with subroutine *NEIGHBOURHOOD2*.

In ABAQUS, this step 3 is performed during the call to subroutine *UEXTERNALDB* ($LOP = 1$). This subroutine with $LOP = 1$ is called at the beginning of each simulation step, but, in this case, an additional condition is checked in order to call *NEIGHBOURHOOD2* only at the beginning of the first step, when every neighbourhood must be defined.

4. **Average of independent variables**

Independent variables (the components of the stress tensor in this case) were stored in the global variable *SDV2* during the execution of previous steps of the bone adaptation simulation.[3] Now, the subroutine *AVERAGE* is called to obtain the averaged independent variables (in ABAQUS, this is done within UMAT subroutine).

5. **Update state variables f_{bm}, d and α**

Next, the subroutine *UPDATE* is called (in ABAQUS, it is done within *UMAT* subroutine). First, the mechanical stimulus σ_{max} is calculated from the averaged stress tensor by following Eq. (8). Then, tables *ttens.txt* and *tcomp.txt* are used to provide the updated f_{bm}, d and α as depicted in Fig. 13. Interpolation of the tables might be necessary.

[3]It is assumed here that we are not running the first step. In this first step, subroutines *AVERAGE* and *UPDATE* are not called (see Fig. 14) and the next step is carried out with predefined initial values.

6. **Update the elastic constants**

   Once the state variables are updated, a constitutive law (Eq. (2) in this case) is used to provide the elastic constants. This is done in subroutine *MECH_PROP* (in ABAQUS, it is done within *UMAT* subroutine).

7. **Update the stiffness and stress tensors**

   Next, the stiffness tensor is updated with the elastic constants calculated in the previous step. Also, the stress tensor must be updated (in ABAQUS, it is done within *UMAT* subroutine), using the just calculated stiffness tensor and the updated strain tensor (in ABAQUS, it is available to *UMAT* as input data).

8. **Update the global variable *SDV1***

   The newly calculated independent variables (the components of the stress tensor in this case) are now saved to the global variable *SDV1*. In contrast to *SDV2*, *SDV1* only contains a temporary copy of the independent variables. This duplication is needed to avoid overwriting *SDV2*, which contains the definitive values of the independent variables.

   The reason for that duplication is the following. If *SDV2* had been overwritten but the FE calculations had not converged for a certain simulation step, this step should start over, from the equilibrium state reached at the end of the previous simulation step. But in such case, the overwritten *SDV2* would not correspond to an equilibrium state and could not be used in *AVERAGE* (step 4 of this procedure).

9. **Copy *SDV1* into *SDV2***

   Only when a simulation step has converged is the temporary *SDV1* copied into the definitive *SDV2* (in ABAQUS, it is done in *UEXTERNALDB* ($LOP = 2$), which is performed at the end of a simulation step. This is the reason for declaring both variables as global, because they must be available from different subroutines).

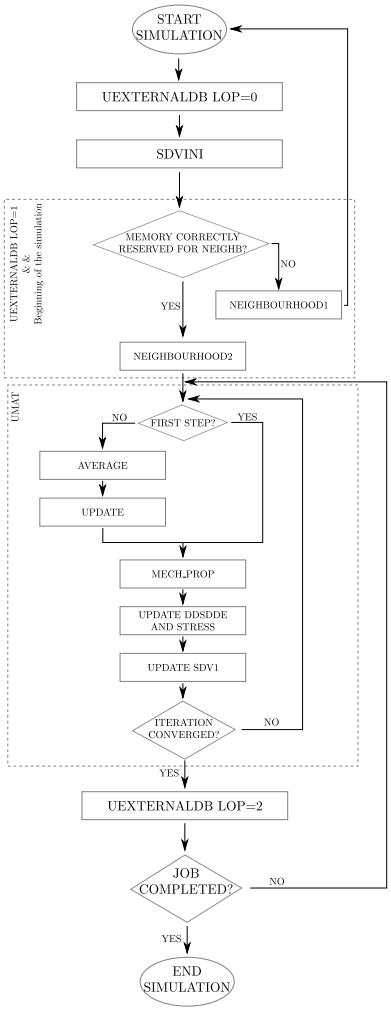

Figure 14: Detailed flowchart of NAM corresponding to the scheme depicted in Fig. 4 if coded.